ACS APPLIED MATERIALS & INTERFACES

Research Article

www.acsami.org

High-Quality Uniaxial $In_xGa_{1-x}N$/GaN Multiple Quantum Well (MQW) Nanowires (NWs) on Si(111) Grown by Metal-Organic Chemical Vapor Deposition (MOCVD) and Light-Emitting Diode (LED) Fabrication

Yong-Ho Ra,[†] R. Navamathavan,[†] Ji-Hyeon Park, and Cheul-Ro Lee*

Semiconductor Materials Process Laboratory, School of Advanced Materials Engineering, Engineering College, Research Center for Advanced Materials Development (RCAMD), Chonbuk National University, Deokjin-dong 664-14, Jeonju 561-756, Korea

ABSTRACT: This article describes the growth and device characteristics of vertically aligned high-quality uniaxial *p*-GaN/$In_xGa_{1-x}N$/GaN multiple quantum wells (MQW)/*n*-GaN nanowires (NWs) on Si(111) substrates grown by metal-organic chemical vapor deposition (MOCVD) technique. The resultant nanowires (NWs), with a diameter of 200−250 nm, have an average length of 2 μm. The feasibility of growing high-quality NWs with well-controlled indium composition MQW structure is demonstrated. These resultant NWs grown on Si(111) substrates were utilized for fabricating vertical-type light-emitting diodes (LEDs). The steep and intense photoluminescence (PL) and cathodoluminescence (CL) spectra are observed, based on the strain-free NWs on Si(111) substrates. High-resolution transmission electron microscopy (HR-TEM) analysis revealed that the MQW NWs are grown along the *c*-plane with uniform thickness. The current−voltage (*I*−*V*) characteristics of these NWs exhibited typical *p*−*n* junction LEDs and showed a sharp onset voltage at 2.75 V in the forward bias. The output power is linearly increased with increasing current. The result indicates that the pulsed MOCVD technique is an effective method to grow uniaxial *p*-GaN/$In_xGa_{1-x}N$/GaN MQW/*n*-GaN NWs on Si(111), which is more advantageous than other growth techniques, such as molecular beam epitaxy. These results suggest the uniaxial NWs are promising to allow flat-band quantum structures, which can enhance the efficiency of LEDs.

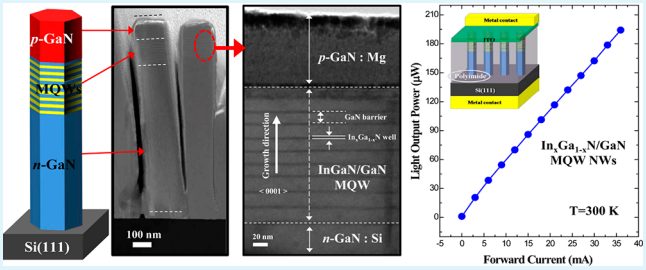

KEYWORDS: *$In_xGa_{1-x}N$/GaN, multiple quantum wells, pulsed flow, MOCVD, uniaxial nanowires, LED structure*

1. INTRODUCTION

III-nitride semiconductors have attracted much attention, especially for their light-emitting device applications, such as highly efficient light-emitting diodes (LEDs) and laser diodes (LDs).[1−6] Although large numbers of commercial products are already available, obtaining high efficiency is still one of the major challenges for the GaN-based optoelectronic devices. The efficiency of $In_xGa_{1-x}N$/GaN-based LEDs is dependent on internal quantum efficiency and the light extraction efficiency. The conventional thin-film technologies have been applied to interfacial lattice mismatch issues that often result in highly defective optical materials.[7−9] In this connection, the unique one-dimensionality inherent to nanowires (NWs) has already solved some of the long-standing technical problems that have been caused by the conventional thin films. In comparison to the conventional thin-film LEDs used today, GaN NWs offer many potential advantages. GaN NWs with a high aspect ratio and large surface-to-volume ratio can dramatically reduce the dislocation density.[10−15] A reduced strain distribution in the nanostructures also leads to a weaker piezoelectric polarization field. Other advantages include large light extraction efficiency and the compatibility with low-cost, large-area silicon substrates.

One of the greatest advantages of these nanostructures is the ability to form axial heterostructures using lattice-mismatched materials, where the formation of interfacial defects can be avoided due to lateral strain relaxation. One-dimensional heterostructure NWs are formed by modulating the growth parameters dynamically. In particular, GaN-related NWs have several features that make them very attractive for optoelectronic device applications.[16−20] One-dimensional nanostructures have many advantages, compared to conventional thin films, including (i) the NW growth is virtually substrate-free, which prevents the formation of threading dislocations, (ii) the alloys of III-nitrides are direct-band-gap semiconductors whose emission wavelength can be easily tuned by varying the alloy compositions, (iii) there are few surface states acting as recombination centers in the band gap of GaN and their alloys are compared to other III−V materials, and (4) GaN NWs can be easily doped to form *p*- and *n*-type materials. Recently, more controlled selective area growth of GaN-based heterostructure NWs were obtained using metal-organic chemical vapor

Received: December 11, 2012
Accepted: February 22, 2013
Published: February 22, 2013

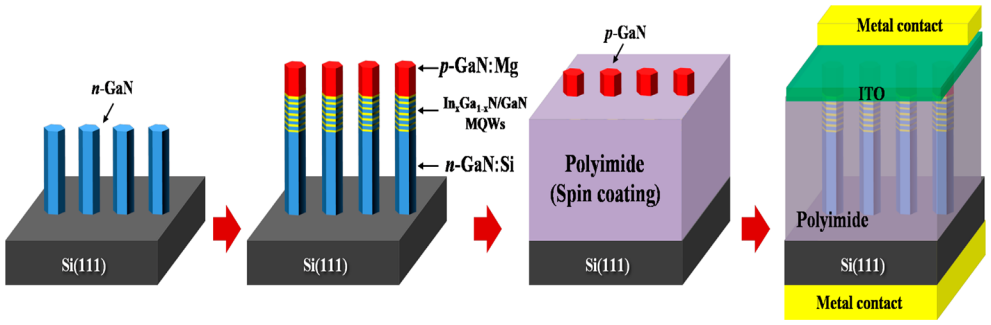

Figure 1. Growth and fabrication sequences of a uniaxial p-GaN/In$_x$Ga$_{1-x}$N/GaN MQW/n-GaN NWs LED structure on Si(111) substrates.

deposition (MOCVD) and molecular beam epitaxy (MBE).[21−23] In GaN NW-based LEDs, a regular arrangement of GaN NWs will be beneficial for device processing. Depending on the GaN-related nanostructures that are achieved, several groups have reported on GaN-based LEDs with different growth and processing methods.[24−27] In this connection, as the principal technique for growing device-quality III-nitrides, the MOCVD method offers the advantages of being inexpensive, having large-scale production, being reproducible, permitting control of precursor delivery, having high purity, and being a simple reactor process, compared to that observed for MBE techniques. Thus, MOCVD is the most promising method for growing III-nitride NWs for nanodevice applications. However, the growth of uniaxial In$_x$Ga$_{1-x}$N/GaN multiple quantum well (MQW) NWs, using MOCVD techniques, was rarely reported. The main purpose of this study is to obtain vertically arranged high-quality MQW structures with well controlled indium composition, to achieve emission at longer wavelength regions. We demonstrate that, by dynamically adjusting the growth parameters, it is possible to obtain uniaxial p-GaN/In$_x$Ga$_{1-x}$N/GaN MQW/n-GaN NWs grown on Si(111) substrates, using a pulsed-flow MOCVD technique.

Herein, we report on the growth and fabrication of vertically aligned GaN NWs-based LED device structures via a combination of conventional and pulsed flow methods, using a MOCVD technique. The resultant NW consists of an p-type GaN at the top, In$_x$Ga$_{1-x}$N/GaN MQW in the middle, and n-GaN at the bottom, as shown in Figure 1. It is shown that p- and n-type doping of the NWs is accomplished with Mg and Si, respectively. The n-type GaN at the bottom of the NWs and the p-type GaN at the top of the NWs serve as electron and hole injection regions, respectively. We optimized various growth parameters to obtain a high-quality NW device structure. The electrical and optoelectronic properties of the p-GaN/In$_x$Ga$_{1-x}$N/GaN MQW/n-GaN NWs have been characterized. Finally, LEDs have been fabricated with an ensemble of NWs, and the characteristics of these devices are also presented.

2. EXPERIMENTAL SECTION

The MQW NWs growth was carried out in a MOCVD system with a horizontal quartz reactor. Figure 1 shows the schematic diagram of the experimental process flow for growing p-GaN/In$_x$Ga$_{1-x}$N/GaN MQW/n-GaN NWs LED device structure on Si(111) substrates. This process involves an axial elongation of nanodroplet-catalyzed growth, followed by controlled heterostructure deposition. The detailed description about the synthesis of Au+Ga nanodroplets has been documented in our previous reports.[28−31] These nanodroplets act as nucleation seeds for the growth of n-GaN NWs in which the Au catalyst that was used no longer existed at the top of the NWs during the vapor−liquid−solid (VLS) process. This will lead to obtaining high-quality LED device structure based on GaN NWs.

First, we grew Si-doped n-type GaN NWs on a Si(111) substrate with Au+Ga nanodroplets at a growth temperature of 950 °C. Trimethylgallium (TMGa) and ammonia (NH_3) were the sources for the gallium and nitrogen, respectively. The In$_x$Ga$_{1-x}$N/GaN MQW NWs were subsequently grown on n-GaN NWs using TMGa, trimethylindium (TMIn), and NH_3 as the sources of gallium, indium, and nitrogen, respectively. For this, we utilized a pulsed- flow precursor method to grow MQW In$_x$Ga$_{1-x}$N and GaN NWs at relatively reduced growth temperatures of 630 and 710 °C, respectively, for different periods. These experiments were repeated to obtain In$_x$Ga$_{1-x}$N/GaN for ∼5, 10, and 15 pairs of wells and barriers of MQW structure. By varying the number of pulses, one can easily tune the period and thickness of the MQW structures. The precursors, TMIn + TMGa and NH_3, were simultaneously allowed into the chamber, for 3 min each. The growth pressure was maintained at 600 Torr. At the final stage, Mg-doped p-type GaN NWs was grown on the top of MQW NWs at a growth temperature of 950 °C.

The morphology of the p-GaN/In$_x$Ga$_{1-x}$N/GaN MQW/n-GaN NWs was analyzed using field-emission scanning electron microscopy (FE-SEM) (Model S-7400, Hitachi, Japan) with an operating voltage of 15 kV. The p-GaN/In$_x$Ga$_{1-x}$N/GaN MQW/n-GaN NWs were removed from the Si(111) substrate, using the sonication process, and then collected on a transmission electron microscopy (TEM) sample grid. The NWs samples for high-resolution transmission electron microscopy (HR-TEM) analysis were prepared by applying a platinum coating to the sample, using a dual-beam focused-ion-beam (FIB, Quanta 3D FEG) technique, with a resolution of 7 nm @ 30 kV and at a beam current of 65 nA. The morphology of NWs was analyzed using the HR-TEM image (Model JEM 2010, JEOL, Japan) at an operating voltage of 200 kV. The band-edge emission of the p-GaN/In$_x$Ga$_{1-x}$N/GaN MQW/n-GaN NWs structures were characterized using PL measurements with a 325-nm line of a He−Cd laser as an excitation source at room temperature. The cathodoluminescence (CL) mapping was performed in a FE-SEM system equipped with a backscattered-electron/CL detector. To study the electrical properties of p-GaN/In$_x$Ga$_{1-x}$N/GaN MQW/n-GaN NW LEDs, a polyimide resist layer was spin-coated to cover the NWs completely. A 100-nm-thick indium tin oxide (ITO) layer was coated on the top surface of the NW, to serve as a transparent electrode and current spreading layer. Thin Au/Ni metal layers were then deposited on both the top and the backside of the Si(111) substrate to serve as p- and n-metal electrode contacts to have good ohmic contact on the samples, as shown in Figure 1. The current−voltage (I−V) and light power−current (L−I) characteristics then were measured for the MQW NW heterostructure, using a semiconductor parameter analyzer (Model 4200-SCS, Keithley Instruments, Cleveland, OH, USA).

3. RESULTS AND DISCUSSION

The GaN-based p-GaN/In$_x$Ga$_{1-x}$N/GaN MQW/n-GaN NW LEDs device fabrication involves the following procedure: initially, the Au catalyst assisted n-type GaN NWs growth,

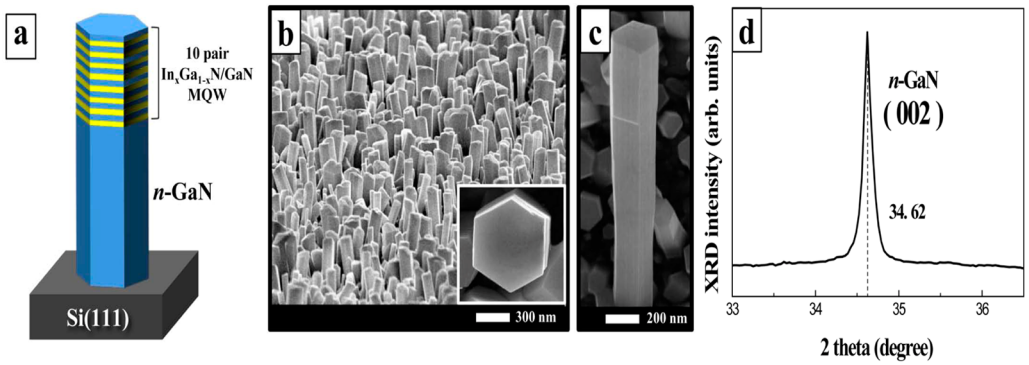

Figure 2. (a) Schematic and (b) tilt-view FE-SEM image of $In_xGa_{1-x}N$/GaN MQW/*n*-GaN NWs grown on Si(111) substrates, inset showing the top view of the NW. (c) FE-SEM image of vertically aligned one single NW. (d) XRD pattern of NWs display diffraction predominantly from the (002) wurtzite peak.

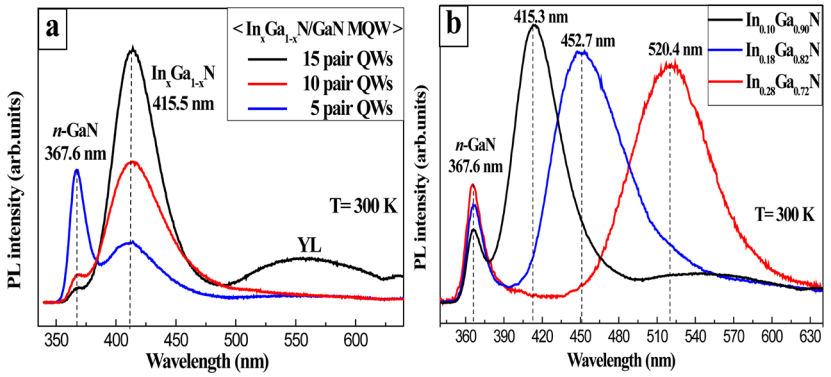

Figure 3. PL spectra of $In_xGa_{1-x}N$/GaN MQW/*n*-GaN NWs (a) with different pairs of MQW and (b) with increasing indium content with 10 pairs of MQW.

followed by sequential pulsed growth of $In_xGa_{1-x}N$/GaN MQW, and, finally, the growth of *p*-type GaN NWs at the top. Figure 2 shows the tilt-view FE-SEM image of the $In_xGa_{1-x}N$/GaN MQW/*n*-GaN NWs grown on Si(111) substrates. Ten (10) pairs of $In_xGa_{1-x}N$/GaN MQW were deposited on *n*-GaN NWs, as shown in Figure 2a. The resultant NWs were very dense, and most of them were vertically aligned on the Si(111) substrate. No significant coalescence and aggregation of individual NWs occurred. The diameters of the $In_xGa_{1-x}N$/GaN MQW/*n*-GaN NWs were observed to be uniform from bottom to top. The inset of Figure 2b shows the well-defined hexagonal-shaped morphology. Figure 2c shows the tilt-view FE-SEM image of a single NW that was vertically aligned to the Si(111) substrate. This result provided the strong evidence that the $In_xGa_{1-x}N$/GaN MQW/*n*-GaN NWs structures were grown along the (0001) direction and was indeed hexagonal faceted at the top end. The diameter of the resultant NWs was observed to vary from 200 nm to 250 nm, with an average length of 2 μm. The NWs have very smooth surface morphology without any nanoparticles. Furthermore, the utilized Au catalyst no longer existed at the top of the NWs during the VLS process, as reported in our previous study,[28] which allows one to obtain a high-quality $In_xGa_{1-x}N$/GaN MQW/*n*-GaN NWs structure. In addition, the X-ray diffraction (XRD) analysis revealed that the prominent diffraction peak from the (002) planes of the wurtzite-type hexagonal GaN NWs indicating that the formed GaN NWs was preferentially oriented in the *c*-axis direction (Figure 2d).

Figure 3 shows the optical properties of fabricated $In_xGa_{1-x}N$/GaN MQW/*n*-GaN NWs grown on Si(111) substrates. To investigate the optical properties, we performed the PL measurement at room temperature. Figure 3a shows the PL spectra of the $In_xGa_{1-x}N$/GaN MQW/*n*-GaN NWs with different pair numbers of the MQW grown on Si(111) substrates. The PL spectra are dominated by the band-edge emission at ~367.6 and 415.5 nm, respectively, corresponding to the GaN and $In_xGa_{1-x}N$ MQW structures. The PL emission intensity increased as the MQW pairs increased. We did not observe emission from any impurity or defect states, except for the $In_xGa_{1-x}N$/GaN MQW with 15 pairs, which typically are observed as a broad band at ~550 nm. The appearance of the yellow luminescence for the MQW with 15 pairs can be associated with vacancy and structural defects, such as stacking faults. Therefore, in our study, we believe that the MQW with 10 pairs can be suitable for the LED device application. At the same time, the PL intensity increased as the MQW pairs increased, which was attributed to the increased amount of incident light absorption with MQW pairs. Furthermore, we performed the PL measurements for 10 pairs of MQW with increasing indium content, to analyze the band-gap properties (Figure 3b). The band-edge emission line width consecutively increases as the In concentration increases. At the same time, it was significantly noted that no defect-related yellow luminescence was observed. The steep and intense PL spectrum with a narrow full width at half-maximum (fwhm) was attributed to the strain-free NWs on Si(111) substrates. However, the fwhm was observed to increase with increasing indium content in the MQW NWs. By suitably varying the indium concentration, one can easily tune the emission wavelength of the MQW NWs. These strain-free NWs can be useful for the fabrication of

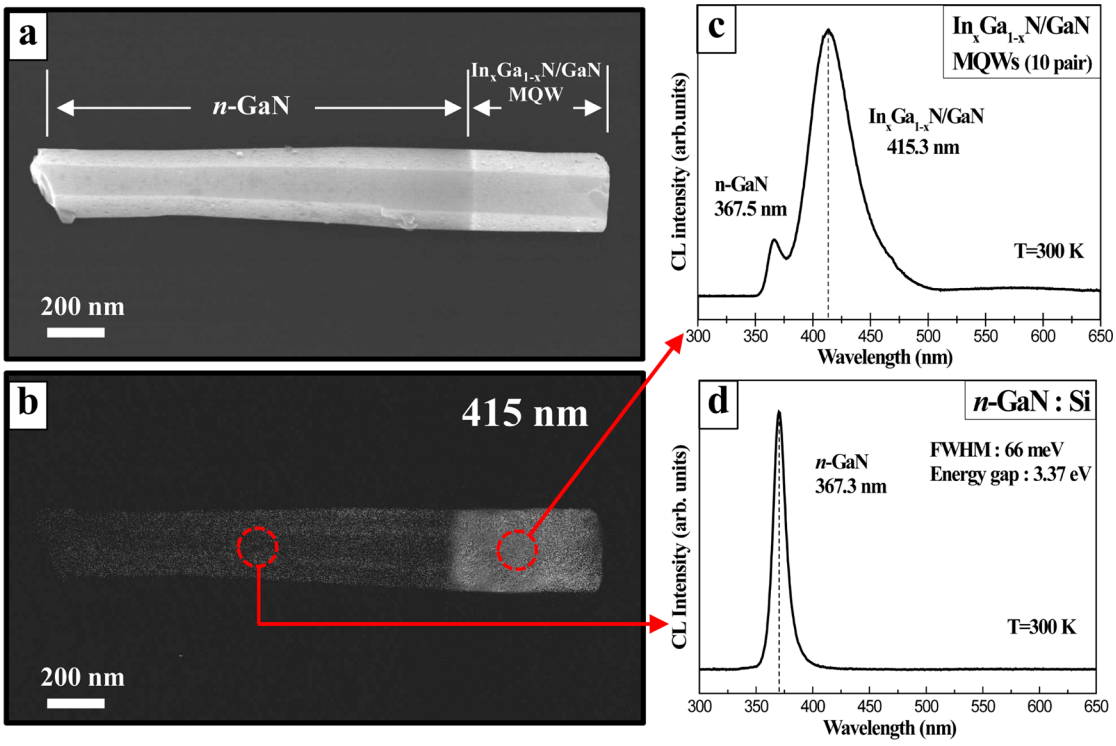

Figure 4. (a) CL mapping image of a single $In_xGa_{1-x}N$/GaN MQW/*n*-GaN NW. (b) Spatially resolved CL mapping at a wavelength of 415 nm. CL spectra taken for (c) $In_xGa_{1-x}N$/GaN MQW and (d) *n*-GaN regions.

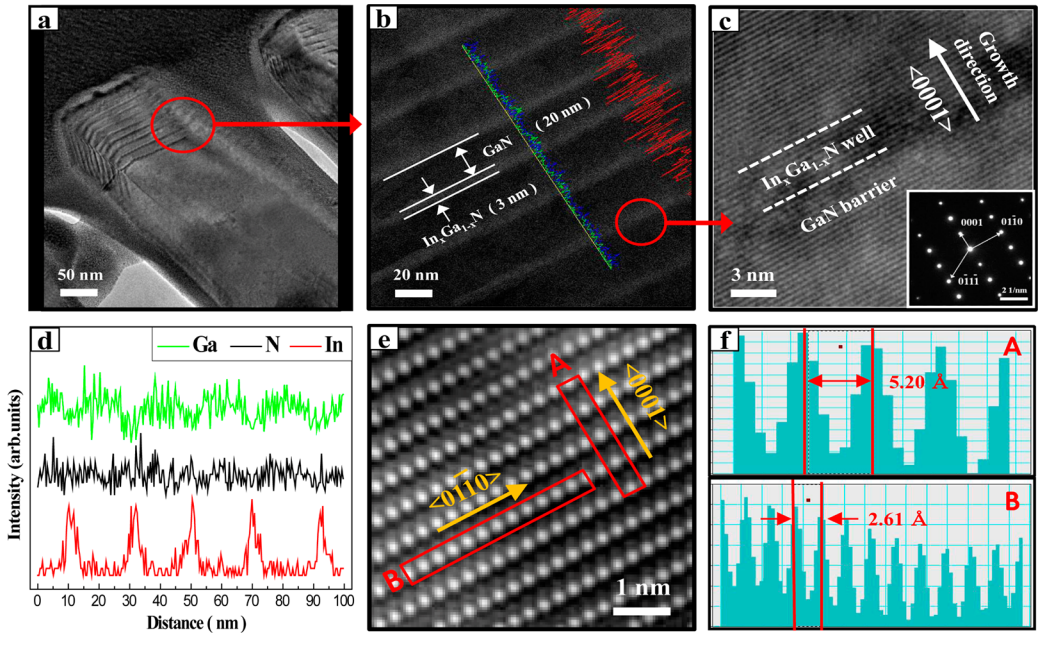

Figure 5. (a) HR-TEM image of $In_xGa_{1-x}N$/GaN MQW NW. (b) ADF-STEM image of the MQW NW. (c) High-magnification lattice image of the MQW NW; the inset shows the corresponding SAED pattern taken along the $\langle 11\bar{2}0 \rangle$ zone axis. (d) HR-TEM EDX spectroscopy of the MQW NW. (e) Inverse fast Fourier transform (IFFT) lattice image of the MQW. (f) Interatomic spacing profiles corresponding to the two regions noted as A and B in panel (e).

compact, efficient, and reliable building blocks for the nanoscale photonic devices.

In order to further clarify the origin of the two band emissions, the wavelength-resolved CL properties of the uniaxial $In_xGa_{1-x}N$/GaN MQW/*n*-GaN NW was investigated. Figure 4 shows the spatially resolved CL mapping image and the spectrum of the individual NW observed at a wavelength of 415 nm. From the CL images, it is seen that the *n*-GaN and MQW structures appeared to be distinct in color, as shown in Figure 4a. The CL mapping image of an $In_xGa_{1-x}N$/GaN MQW structure recorded at a wavelength of 415 nm appeared to be more luminescent, compared to that of the *n*-GaN counterpart, which appeared to be transparent, as shown in Figure 4b. The respective CL profile recorded at two different

dx.doi.org/10.1021/am303056v | ACS Appl. Mater. Interfaces 2013, 5, 2111−2117

regions observed at a wavelength 415 nm corresponds to the maximum peak energy of the two band emissions. The CL spectra, as presented in Figures 4c and 4d, were dominated by the band-edge emission at 415.3 and 367.5 nm, corresponding to $In_xGa_{1-x}N$/GaN and *n*-GaN structures, respectively. These results demonstrate that the CL emission intensity of the two structures (367.5 and 415.3 nm, corresponding to *n*-GaN and $In_xGa_{1-x}N$/GaN MQW, respectively) are quite uniform, which might be related to the homogeneous distribution of defect-free and vertically aligned $In_xGa_{1-x}N$/GaN MQW/*n*-GaN NW. These CL data slightly differ from the PL data, since the CL spectrum was observed for a single NW structure. The narrow band emission of the individual NW obtained from the CL spectrum indicates that the related GaN NWs have good crystal quality. The CL data clearly confirms the continuous emission intensity on the $In_xGa_{1-x}N$/GaN MQW/*n*-GaN NW without any defects, which is highly efficient for the LED device applications.

The $In_xGa_{1-x}N$/GaN MQW/*n*-GaN NW was further revealed by cross-sectional HR-TEM and EDX mapping. Figure 5a shows an HR-TEM image of the MQW NW grown on *n*-GaN NWs on Si(111) substrates. The MQW NWs were uniformly grown along the *c*-plane. To check the MQW structure clearly, high-angle annular dark-field (ADF) images were recorded with a scanning transmission electron microscopy (STEM) system. The $In_xGa_{1-x}N$/GaN MQW structure is clearly seen and is equally distributed on the *n*-GaN NW, as shown in Figure 5b. It was observed that the thickness of the $In_xGa_{1-x}N$/GaN MQW NW were almost uniform throughout the periods. The thicknesses of the $In_xGa_{1-x}N$ and GaN MQW are determined to be 3 and 20 nm, respectively. The possibility to grow a well-defined 3-nm-thick $In_xGa_{1-x}N$ layer in the MQW structure suggests that it will be feasible to control the sharply defined quantum well structures. Therefore, the pulsed-flow method provides a clear formation of the $In_xGa_{1-x}N$/GaN MQW interface with growth cycles. Figure 5c shows a cross-sectional HR-TEM lattice image of the MQW NW. This images shows the [0001] growth direction of a MQW NW, which was aligned along the NW axis (*c*-plane). A representative selected-area electron diffraction (SAED) pattern taken along the $\langle 11\bar{2}0\rangle$ zone axis is shown in the inset of Figure 5c, where (0001), $(01\bar{1}0)$, and $(0\bar{1}1\bar{1})$ diffraction spots were present. The clear SAED spots indicated that the SAED paatern was of a high-quality hexagonal-structure $In_xGa_{1-x}N$/GaN MQW NW. There are no extended defects, such as misfit dislocations and stacking faults observed in the $In_xGa_{1-x}N$/GaN MQW NW structure. It is evident that the MQW structure changes abruptly, although there is some atomic mixing near the interface, which is not observed for the sharper interface between the well and the barrier. A HR-TEM energy-dispersive X-ray spectroscopy (EDX) line profile of the $In_xGa_{1-x}N$/GaN MQW NW region clearly confirmed the spatial distributions of elemental Ga, In, and N in the different regions along the growth direction of the NW LED structure, as shown in Figure 5d. A clearer lattice image is shown in Figure 5e, which was taken from the inverse fast Fourier transform (IFFT) image. The interplanar spacing of the $\langle 0001\rangle$ and $\langle 01\bar{1}0\rangle$ plane NW segments, measured from the TEM image, were ~5.19 and 2.61 Å, respectively, as shown in Figure 5f. The wurtzite crystal structure in the MQW NWs was confirmed in both diffraction patterns and HR-TEM images.

Figure 6 shows the morphology of a fabricated *p*-GaN/$In_xGa_{1-x}N$/GaN MQW/*n*-GaN NW LED device structure.

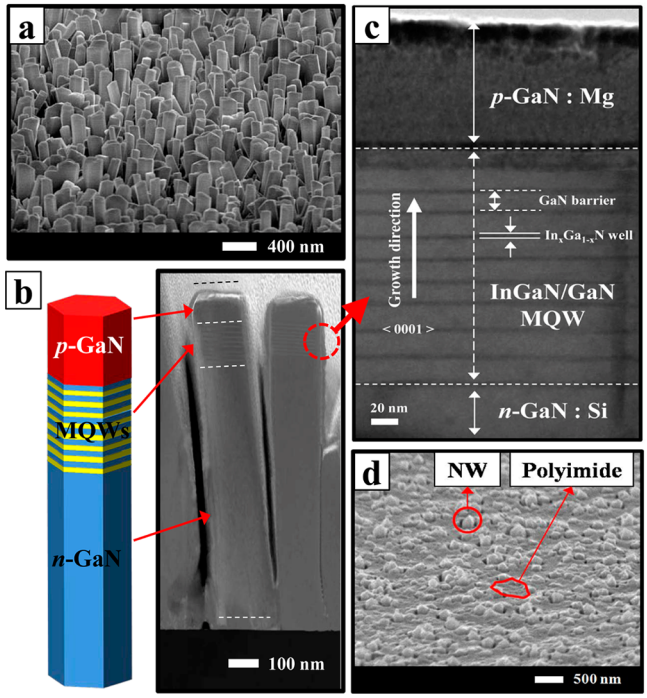

Figure 6. Morphology of fabricated *p*-GaN/$In_xGa_{1-x}N$/GaN MQW/*n*-GaN NW LEDs device structure: (a) tilt-view FE-SEM; (b) schematic and low-magnification HR-TEM image; (c) high-magnification HR-TEM image of the region noted in panel (b); and (d) tilt-view FE-SEM image of a partially etched polyimide spin-coated on top of the NWs.

Figure 6a shows the tilt-view FE-SEM image of the complete NW LED device structure after growing *p*-GaN NWs. The shape of the NW LED structure was unaltered, even after the growth of *p*-GaN NWs on the top of the MQW NWs. Figures 6b and 6c show low- and high-magnification HR-TEM images of a *p*-GaN/$In_xGa_{1-x}N$/GaN MQW/*n*-GaN NW LED device structure with 10 pairs of MQW grown on a Si(111) substrate. This morphological analysis clearly revealed that the NW is vertical and grew perpendicular along the *c*-axis ($\langle 0001\rangle$) with very sharp interfaces. The bottom and top sections of the NWs were doped *n*-type and *p*-type, using Si and Mg, respectively. The NW-array LED device was then spin-coated with a polyimide layer and partially etched, as shown in Figure 6d. After the top side of the polyimide layer was etched, the NWs were clearly visible, as indicated in Figure 6d. The active region of the LED device consists of 10 vertically aligned $In_xGa_{1-x}N$ NWs with a thickness of 3 nm, which were well-separated by 20-nm GaN barrier NWs. Overall, these HR-TEM, PL, CL and EDX profile, and ADF image studies demonstrate that the growth of the *p*-GaN/$In_xGa_{1-x}N$/GaN MQW/*n*-GaN NW LED device structure on Si(111) substrates was well-controlled by means of the sequence, thickness, and compositions.

Finally, the electrical properties of the *p*-GaN/$In_xGa_{1-x}N$/GaN MQW/*n*-GaN NWs LED fabricated on Si(111) substrates were determined. To inject holes and electrons simultaneously into the MQW NWs, the metal contacts were deposited onto the NWs at the top and bottom of the Si(111) substrates. Figure 7 shows the room-temperature *I*−*V* characteristics of this NW LED, which is schematically shown in the inset. The measured *I*−*V* characteristics at room temperature showed a sharp onset voltage at 2.75 V in the forward bias, with relatively negligible leakage currents at the reverse bias. From the *I*−*V*

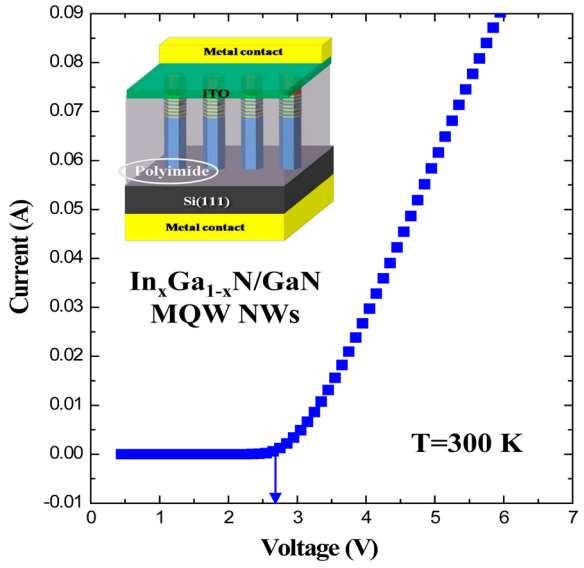

Figure 7. *I*–*V* characteristics of *p*-GaN/$In_xGa_{1-x}N$/GaN MQW/*n*-GaN NW LED structure grown and fabricated on Si(111) substrates. The fabricated LED device on a Si(111) substrate is schematically displayed in the inset.

curve, the current linearly increased as the applied voltage increased: 20 mA at 4.0 V, 60 mA at 5 V, and 80 mA at 6 V. The electrical transport measurements demonstrate that these vertical NWs exhibit well-defined and reliable electrical *n*-type and *p*-type materials and behave as *p*–*n* diodes. In Figure 8, the

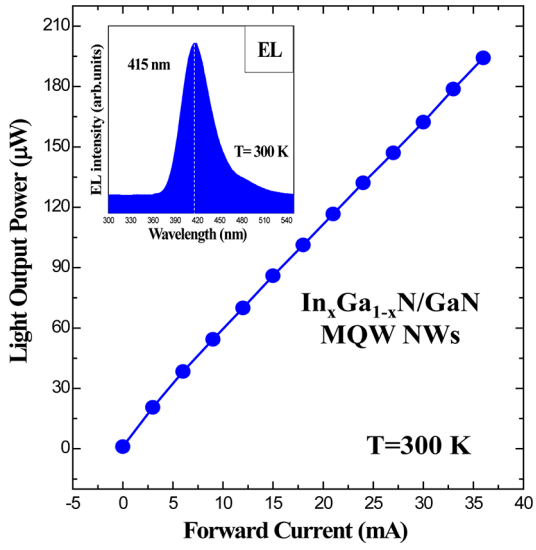

Figure 8. Light output power of *p*-GaN/$In_xGa_{1-x}N$/GaN MQW/*n*-GaN NW LED, as a function of current. Inset shows the electroluminescence (EL) spectrum of light emission.

light output power values of the MQW NW LEDs was studied as a function of current. The output power linearly increased as the current increased. The linear enhancement of output power could be attributed to the highly uniform and defect-free $In_xGa_{1-x}N$/GaN MQW NW structure. The output power curve exhibited a gradual increase with increasing current, which was observed to be 60 μW at 10 mA, 110 μW at 20 mA, and 188 μW at 35 mA. The electroluminescence (EL) spectrum of the emitted light is shown in the inset of Figure 8. Our single *p*-GaN/$In_xGa_{1-x}N$/GaN MQW/*n*-GaN NWs *p*-*n* junction LED are composed of a single epitaxial growth, which can control one-dimensional current transport through the single NW. The low-temperature growth of *p*-GaN NWs at 950 °C was very promising for effectively suppressing the interdiffusion and re-evaporation of indium in the $In_xGa_{1-x}N$/GaN MQW with a high indium content (415 nm) for green LEDs, which is in good agreement with the PL and CL data. The ability to grow a vertically aligned MQW NWs structure with diameter control will provide exciting electronic and optoelectronic properties, which can be utilized for future devices. Further investigation is required to improve the electrical characteristics of the uniaxially based NW LED device by considering and optimizing the carrier concentration of *p*- and *n*-type GaN NWs, the thickness of the barrier and well structure, and the electrical contacts to the NWs; such studies are now underway.

4. CONCLUSIONS

We have fabricated vertically aligned *p*-GaN/$In_xGa_{1-x}N$/GaN MQW/*n*-GaN NWs LED structures on Si(111) substrates via a combination of conventional and pulsed-flow methods, using a metal-organic chemical vapor deposition (MOCVD) technique. The successful growth of LED device structures was achieved with different periods of MQW structures with uniform diameter. The diameter of the resultant NWs was observed to vary from 200 nm to 250 nm, with an average length of 2 μm. The surface morphology, optical characterization, and electrical characterization of the fabricated *p*-GaN/$In_xGa_{1-x}N$/GaN MQW/*n*-GaN NWs LED structures were studied via field-emission scanning electron microscopy (FE-SEM), high-resolution transmission electron microscopy (HR-TEM), photoluminescence (PL), cathodoluminescence (CL), current–voltage (*I*–*V*), and light output power–current (*L*–*I*) measurements. The results of PL and CL evidenced that the grown $In_xGa_{1-x}N$/GaN MQW NWs were of good optical quality with few defects. The *p*-GaN/$In_xGa_{1-x}N$/GaN MQW/*n*-GaN NWs LED showed a current rectification with a sharp onset voltage at 2.75 V in the forward bias. The output power of the NW LED linearly increased as the current increased. The linear enhancement of output power could be attributed to the highly uniform and defect-free *n*-GaN NW and $In_xGa_{1-x}N$/GaN MQW NW structures. Electrical transport measurement demonstrates that these NWs exhibited well-defined and reliable behavior of *p*–*n* junction diodes. These findings have addressed that these uniaxial MQW NWs are promising to allow the flat-band quantum structures, which can enhance the efficiency of LEDs.

AUTHOR INFORMATION

Corresponding Author

*Tel.: +82-63-270-2304. Fax: +82-63-270-2305. E-mail: crlee7@jbnu.ac.kr.

Author Contributions

†These authors contributed equally to this work.

Notes

The authors declare no competing financial interest.

ACKNOWLEDGMENTS

This research was supported by the National Research Foundation of Korea (NRF) grant funded by the Korea Government (MEST) (BRL. No. 2010-0019626) and by the Basic Research of the Korea Science and Engineering

Foundation (NRL. R0A-2008-000-0031-0) of Korean Government (MOEHRD). This research was also financially supported by the Ministry of Education, Science and Technology (MEST) and National Research Foundation of Korea (NRF) through the Human Resource Training Project for Regional Innovation.

REFERENCES

(1) Lin, Y. D.; Chakraborty, A.; Brinkley, S.; Kuo, H. C.; Melo, T.; Fujito, K.; Speck, J. S.; DenBaars, S. P.; Nakamura, S. *Appl. Phys. Lett.* **2009**, *94*, 261108-1−261108-3.
(2) Lee, J. W.; Sone, C.; Park, Y.; Lee, S. N.; Ryu, J. H.; Dupuis, R. D.; Hong, C. H.; Kim, H. *Appl. Phys. Lett.* **2009**, *95*, 011108-1−011108-3.
(3) Kuo, Y. K.; Chang, J. Y.; Tsai, M. C.; Yen, S. H. *Appl. Phys. Lett.* **2009**, *95*, 011116-1−011116-3.
(4) Schubert, E. F.; Kim, J. K. *Science* **2005**, *308*, 1274−1278.
(5) Farrell, R. M.; Haeger, D. A.; Hsu, P. S.; Schmidt, M. C.; Fuijito, K.; Feezell, D. F.; DenBaars, S. P.; Speck, J. S.; Nakamura, S. *Appl. Phys. Lett.* **2011**, *99*, 171113−1−171113−3.
(6) Gradecak, S.; Qian, F.; Li, Y.; Park, H. G.; Lieber, C. M. *Appl. Phys. Lett.* **2005**, *87*, 173111-1−173111-3.
(7) Schubert, E. F. *Light Emitting Diodes*; Cambridge University Press: New York, 2003.
(8) Meneghini, M.; Barbisan, D.; Bilenko, Y.; Shataly, M.; Yang, J.; Gaska, R.; Meneghesso, G.; Zanoni, E. *Microelectron. Reliab.* **2010**, *50*, 1538−1542.
(9) Mills, A. *III-Vs Rev.* **2001**, *14*, 32−37.
(10) Hersee, S. D.; Sun, X.; Wang, X. *Nano Lett.* **2006**, *6*, 1808−1811.
(11) Lin, C.; Yu, G.; Wang, Z.; Cao, M.; Lu, H.; Gong, H.; Qi, M.; Li, A. *J. Phys. Chem. C* **2008**, *112*, 18821−18824.
(12) Ra, Y. H.; Navamathavan, R.; Cha, J. H.; Song, K. Y.; Lim, H. C.; Park, J. H.; Kim, D. W.; Lee, C. R. *Jpn. J. Appl. Phys.* **2010**, *49*, 045004−1−045004−4.
(13) Schuster, F.; Furtmayr, F.; Zamani, R.; Magan, C.; Morante, J. R.; Arbiol, J.; Garrido, J. A.; Stutzmann, M. *Nano Lett.* **2012**, *12*, 2199−2204.
(14) Dick, K. A. *Prog. Cryst. Growth Charact. Mater.* **2008**, *54*, 138−173.
(15) Hayden, O.; Agarwal, R.; Liu, W. *Nano Today* **2008**, *3*, 12−22.
(16) Li, S.; Waag, A. *J. Appl. Phys.* **2012**, *111*, 071101−1−071101−23.
(17) Weisse, J. M.; Lee, C. H.; Kim, D. R.; Zhang, X. *Nano Lett.* **2012**, *12*, 3339−3343.
(18) Rigutti, L.; Tchernycheva, M.; Bugallo, A. D. L.; Jacopin, G.; Julien, F. H.; Zagonel, L. F.; March, K.; Stephan, O.; Kociak, M.; Songmuang, R. *Nano Lett.* **2010**, *10*, 2939−2943.
(19) Posada, F. G.; Songmuang, R.; Hertog, M. D.; Monroy, E. *Nano Lett.* **2012**, *12*, 172−176.
(20) Wierer, J. J.; Li, Q.; Koleske, D. D.; Lee, S. R.; Wang, G. T. *Nanotechnology* **2012**, *23*, 194007.
(21) Yeh, T. W.; Lin, Y. T.; Stewart, L. S.; Dapkus, P. D.; Sarkissian, R.; Obrien, J. D.; Ahn, B.; Nutt, S. R. *Nano Lett.* **2012**, *12*, 3257−3262.
(22) Carnevale, S. D.; Yang, J.; Phillips, P. J.; Mills, M. J.; Myers, R. C. *Nano Lett.* **2011**, *11*, 866−871.
(23) Nguyen, H. P. T.; Zhang, S.; Cui, K.; Hui, X.; Han, X.; Fathololoumi, S.; Couillard, M.; Botton, G. A.; Mi, Z. *Nano Lett.* **2011**, *11*, 1919−1924.
(24) Kim, H. M.; Cho, Y. H.; Lee, H.; Kim, S. I.; Ryu, S. R.; Kim, D. Y.; Kang, T. W.; Chung, K. S. *Nano Lett.* **2004**, *6*, 1059−1064.
(25) Dick, K. A.; Bolinsson, J.; Borg, B. M.; Johansson, J. *Nano Lett.* **2012**, *12*, 3200−3206.
(26) Guo, W.; Zhang, M.; Banerjee, A.; Bhattacharya, P. *Nano Lett.* **2010**, *10*, 3355−3359.
(27) Yeh, T. W.; Lin, Y. T.; Ahn, B.; Stewart, L. S.; Dapkus, P. D.; Nutt, S. R. *Appl. Phys. Lett.* **2012**, *100*, 033119-1−033119-3.
(28) Ra, Y. H.; Navamathavan, R.; Park, J. H.; Song, K. Y.; Lee, Y. M.; Kim, D. W.; Jun, B. B.; Lee, C. R. *Jpn. J. Appl. Phys.* **2010**, *49*, 091003-1−091003-5.
(29) Navamathavan, R.; Ra, Y. H.; Song, K. Y.; Kim, D. W.; Lee, C. R. *Current Appl. Phys.* **2011**, *11*, 77−81.
(30) Jang, E. S.; Ra, Y. H.; Lee, Y. M.; Yun, S. H.; Kim, D. W.; Navamathavan, R.; Kim, J. S.; Lee, I. H.; Lee, C. R. *Jpn. J. Appl. Phys.* **2009**, *48*, 091001-1−091001-4.
(31) Ra, Y.-H.; Navamathavan, R.; Lee, C.-R. *CrystEngComm* **2012**, *14*, 8208−8214 (DOI: 10.1039/C2CE26281A).